Central Lancashire Online Knowledge (CLoK)

Title	Acid Dissociation of 3-Mercaptopropionic Acid Coated CdSe–CdS/Cd0.5Zn0.5S/ZnS Core–Multishell Quantum Dot and Strong Ionic Interaction with Ca2+ Ion
Type	Article
URL	https://clok.uclan.ac.uk/20612/
DOI	https://doi.org/10.1021/acs.jpcc.5b11023
Date	2016
Citation	Shambetova, Nestan, Chen, Yun, Xu, Hao, Li, Li, Solandt, Johan, Zhou, Yuhua, Wang, Jingbo, Su, Haibin, Brismar, Hjalmar et al (2016) Acid Dissociation of 3-Mercaptopropionic Acid Coated CdSe–CdS/Cd0.5Zn0.5S/ZnS Core–Multishell Quantum Dot and Strong Ionic Interaction with Ca2+ Ion. The Journal of Physical Chemistry C, 120 (6). pp. 3519-3529. ISSN 1932-7447
Creators	Shambetova, Nestan, Chen, Yun, Xu, Hao, Li, Li, Solandt, Johan, Zhou, Yuhua, Wang, Jingbo, Su, Haibin, Brismar, Hjalmar and Fu, Ying

It is advisable to refer to the publisher's version if you intend to cite from the work.
https://doi.org/10.1021/acs.jpcc.5b11023

For information about Research at UCLan please go to http://www.uclan.ac.uk/research/

Acid Dissociation of 3-Mercaptopropionic Acid Coated CdSe−CdS/Cd$_{0.5}$Zn$_{0.5}$S/ZnS Core−Multishell Quantum Dot and Strong Ionic Interaction with Ca^{2+} Ion

Nestan Shambetova,[†] Yun Chen,[‡] Hao Xu,[†] Li Li,[†] Johan Solandt,[†,§] Yuhua Zhou,[∥] Jingbo Wang,[∥] Haibin Su,[⊥] Hjalmar Brismar,[†] and Ying Fu*,[†]

[†]Science for Life Laboratory, Department of Applied Physics, Royal Institute of Technology, SE-10691 Stockholm, Sweden

[‡]Department of Molecular and Clinical Medicine/Clinical Physiology, The Sahlgrenska Academy and University Hospital, University of Gothenburg, SE-41345 Gothenburg, Sweden

[§]AstraZeneca R&D, SE-43183 Mölndal, Sweden

[∥]UCLan Biomedical Technology (Shenzhen) Ltd., University of Central Lancashire, Shenzhen Virtual University Park Building No. 19, Shenzhen, 518057, China

[⊥]School of Materials Science, Nanyang Technological University, 50 Nanyang Avenue, 639798, Singapore, Singapore

ABSTRACT: By devising careful electrophoresis, it was shown that at pH below 7.0, the electrophoretic mobility of 3-mercaptopropionic acid (3MPA) coated CdSe−ZnS core−shell quantum dots (denoted as QD-3MPA) was very small. At pH above 7.0, QD-3MPA migrated toward the anode, implying acid dissociation, and the degree of which was proportional to the pH value. QD-3MPA's electrophoretic mobility was impaired after adding sufficient Ca^{2+} ions to the QD solution and revived when a similar amount of Ca^{2+} chelators (ethylene glycol tetraacetic acid, EGTA) was added. This demonstrated that acid dissociation and its pH dependence of 3MPA on the QD surface are critical factors in understanding the electric and optical properties of QDs.

The acid dissociated QD-3MPA interacted strongly with Ca^{2+}, forming a charge neutral QD-3MPA−Ca^{2+} complex in the absence of EGTA. First-principles study confirmed the observed experimental evidence. The strong ionic interaction between acid dissociated QD-3MPA and Ca^{2+} is critical for developing reliable QD-based biosensing assays. Moreover, the strategy and techniques reported in this work are easily applicable to other fluorescent biomarkers and therefore can be important for advancing *in vivo* and *in vitro* imaging, sensing, and labeling.
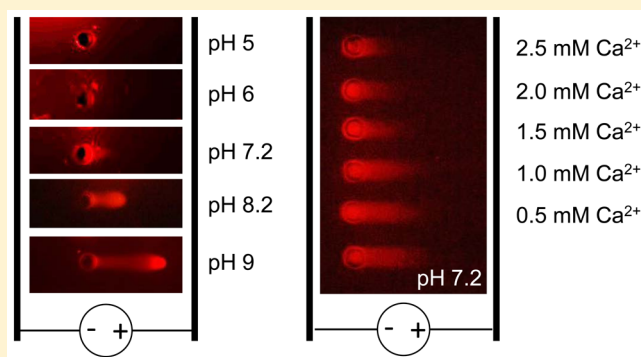
INTRODUCTION

Colloidal quantum dots (QDs) have been extensively studied and developed for many applications, including solar cells,[1,2] bioimaging[3,4] and biosensing.[5,6] Many studies show that the fluorescence intensity of QDs was decreased (quenched) with the addition of free ions such as Zn^{2+}, Cu^{2+}, Ag$^+$, Fe^{3+}, Hg^{2+}, Na$^+$, K$^+$, and Ca^{2+}[6−14] to the QD solution, leading to the potential for QD-based ion sensor development. It was reported that the fluorescence intensity of water-dispersible CdSe−CdS/ZnS core−multishell QDs coated with 3-mercaptopropionic acids (3MPA, HSCH$_2$CH$_2$CO$_2$H) was inversely and reversibly associated with the concentration of free Ca^{2+} ions in the QD solution (pH = 7.2).[15]

The pH value of the QD solution is known to greatly influence the fluorescence spectra of mercaptoacetic acid (MAA, HSCH$_2$CO$_2$H) coated QDs, even QDs embedded in polymer microcapsules; see, e.g., refs 16−18. Moreover, the pH effect was found to be reversible in the pH range between 6 and 9.[18] MAA-coated ZnS-capped CdSe QDs[16] and MAA-coated

CdTe QDs[17] were reported to be highly fluorescent at high pH, while high fluorescence at pH = 6 and low at pH = 9 from MAA-stabilized CdTe QDs were also reported.[18] Fluorescence intensity and lifetime of cysteamine- (HSCH$_2$CH$_2$NH$_2$-) capped CdTeSe-ZnS core−shell QDs were shown to decrease at low pH values.[19]

Two critical issues arise here, the first of which concerns the physical and chemical nature of the surface ligands on the QD surface at different pH values, and the second of which regards the interactions between free ions and QDs, in order to understand the experimental observations. They are also among the first questions we must fully understand before putting QDs into any *in vitro* and/or an *in vivo* bio system. In this work we attempted to find experimental and theoretical means to illuminate these issues by studying 3MPA-coated CdSe−CdS/

Cd$_{0.5}$Zn$_{0.5}$S/ZnS core−multishell QDs, denoted simply as QD-3MPA.

Hg^{2+}-induced QD aggregation was proposed to explain the reduction of QD fluorescence intensity in the presence of Hg^{2+} ions.[20] This aggregation may not effectively explain the reported reversible modification of QD fluorescence properties induced by adding and removing Ca^{2+} to and from the QD solutions since characteristic fluorescence blinking of single QDs was still observed in the presence of Ca^{2+} ions, i.e., QDs remained single in the presence of Ca^{2+} ions.[15] Early theoretical studies showed that a free Ca^{2+} ion can interact with QD-3MPA via Coulombic interaction, fixing QD-3MPA and Ca^{2+} as one complex, denoted as QD-3MPA−Ca^{2+}.[15] However, the stability of such a complex has not been confirmed experimentally. One possible experimental method is to measure the temperature effect since collisional quenching depends strongly on the temperature due to thermal motions of the collision partners. However, QD fluorescence intensity depends also on the temperature.[21,22] Novel experimental methods are therefore to be devised to unravel the microscopic nature of the interaction between Ca^{2+} and QD-3MPA.

Electrophoresis is widely used in biochemistry to separate molecules according to their sizes and charges. It has also been used in studying colloidal QDs.[4,23−25] QD fluorescence lifetime measurement was analyzed to study the microscopic exciton states of the QD.[26] It was also used to measure pK_a of cysteamine capped CdTeSe−ZnS core−shell QDs.[19] In this work, we studied the nature of the QD-3MPA surface and the interaction between Ca^{2+} and QD-3MPA using electrophoresis, QD fluorescence and its lifetime measurement, and first-principles study. The basic hypothesis is as follows: Acid dissociated QD-3MPA is expected to be negatively charged and its migration toward the anode should depend upon the degree of acid dissociation of 3MPA on the QD surface. If Ca^{2+} interacts strongly with acid dissociated QD-3MPA to form a stable QD-3MPA−Ca^{2+} complex, the QD-3MPA−Ca^{2+} complex should be less negatively charged, and its migration toward the anode is expected to be slower than that of QD-3MPA. However, if the interaction between Ca^{2+} and QD-3MPA is largely collisional, the addition of Ca^{2+} will not significantly affect the electrophoretic mobility of QD-3MPA. The charges resulting from acid dissociation and binding with Ca^{2+} and their distribution on the QD surface will affect the exciton states of the QD and therefore be reflected in the QD fluorescence intensity and lifetime spectra.

■ MATERIALS AND METHODS

QD Samples. Water-dispersible CdSe−CdS/Cd$_{0.5}$Zn$_{0.5}$S/ZnS core−multishell QDs were fabricated in-house using common recipes.[27] Standard structure characterizations including core, shell, QD size distribution and surface ligands of these QDs have been performed, and details were published; see, e.g., refs 28 and 29. Consisting of a CdSe core, a CdS shell of 2 monolayers, another shell of 1 monolayer Cd$_{0.5}$Zn$_{0.5}$S, and 1.5 monolayer ZnS, these QDs were coated with 3MPA surface ligands and had fluorescence peaks around 600 nm at room temperature. The peak wavelength varied slightly from different growth batches and different QDs were denoted by their fluorescence peak wavelengths such as QD600 denotes QDs with a fluorescence peak at 600 nm. Our QDs were dispersed in 4-(2-hydroxyethyl)-1-piperazineethanesulfonic acid (HEPES) buffer containing 50 mM HEPES and 23 mM NaOH at pH = 7.2. Figure 1a shows one transmission electron microscope
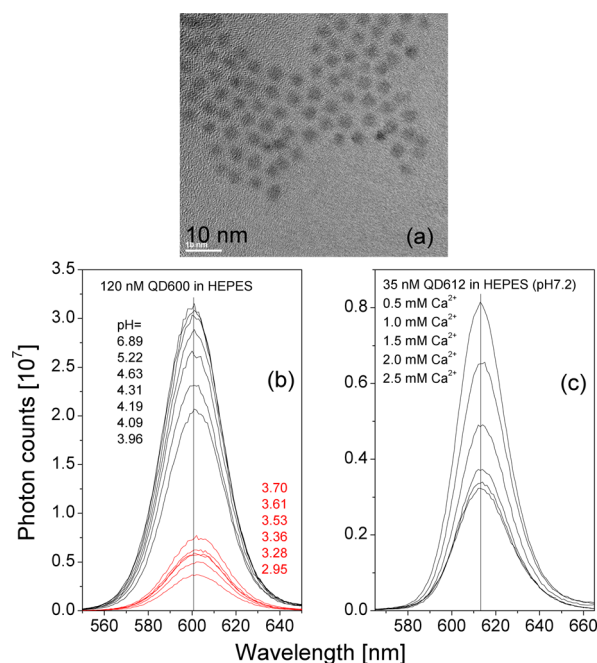

Figure 1. Characterization of 3MPA-coated CdSe−CdS/Cd$_{0.5}$Zn$_{0.5}$S/ZnS core−multishell QDs. (a) Transmission electron microscope (TEM) image of the QDs (QD600). (b) Fluorescence spectra of QD600 at different pH values. (c) Fluorescence spectra of the six QD612 samples (without and with Ca^{2+}). Fluorescence spectra were excited by a 400 nm laser beam and measured at room temperature.

(TEM) image of QD600 and the fluorescence spectra are presented in parts b (QD600 at different pH values) and c (QD612 in the presence of Ca^{2+} ions). The QD size of each growth batch was uniform with a standard deviation of about 0.5 nm. The full width at half-maximum (fwhm) of the QD fluorescence peaks was approximately 25 nm, which was shown to be intrinsic in the fluorescence of colloidal QDs.[26]

The pH value of the QD solution was modified by adding HCl or NaOH, while stock solutions of Ca^{2+} (1 M CaCl$_2$) and 0.5 M EGTA were prepared in the HEPES buffer. A small volume of Ca^{2+} stock solution was injected into five of six 0.5 mL Eppendorf tubes (each containing 0.3 mL of QD solution) to reach final Ca^{2+} concentrations of 0.5, 1.0, 1.5, 2.0, and 2.5 mM, respectively. For example, 0.15 μL of 1 M Ca^{2+} stock solution was added to the 0.3 mL QD solution to attain 0.5 mM Ca^{2+}, making the volume change of the QD solution negligible after adding Ca^{2+}. The six Eppendorf tubes were shaken first by hand then placed on a Heidolph Reax 2000 shaker at speed 2 so that the contents were thoroughly mixed. Afterward, the samples were incubated at room temperature for 30 min to ensure that the interactions between QD-3MPA and Ca^{2+} were completed before fluorescence and electrophoresis experiments. The six QD samples were denoted as

- **1**: 35 nM QD-3MPA
- **2**: 35 nM QD-3MPA + 0.5 mM Ca^{2+}
- **3**: 35 nM QD-3MPA + 1.0 mM Ca^{2+}
- **4**: 35 nM QD-3MPA + 1.5 mM Ca^{2+}
- **5**: 35 nM QD-3MPA + 2.0 mM Ca^{2+}
- **6**: 35 nM QD-3MPA + 2.5 mM Ca^{2+}

The fluorescence spectra of QD samples were measured by an optical spectrometer (FluoroMax-3 Horiba Jobin Yvon) and are presented in Figure 1, parts b and c. As earlier reported, the QD fluorescence depended on the pH value of the QD solution

as well as the concentration of Ca^{2+} ions. Note that the QD fluorescence peak wavelength was modified by the pH value but remained largely unchanged when Ca^{2+} ions were introduced.

To study the cross interactions of QD-3MPA, Ca^{2+}, and EGTA, another six Eppendorf tubes of QD-3MPA with and without Ca^{2+} were first prepared as before. EGTA stock solution was then added into the five samples containing Ca^{2+} to reach final EGTA concentrations of 0.5, 1.0, 1.5, 2.0, and 2.5 mM, respectively. The six samples were thoroughly mixed, then incubated at room temperature for 1 h before electrophoresis experiments. These six QD samples were denoted as

- **1**: 35 nM QD-3MPA (the same sample 1)
- **2′**: 35 nM QD-3MPA + 0.5 mM Ca^{2+} + 0.5 mM EGTA
- **3′**: 35 nM QD-3MPA + 1.0 mM Ca^{2+} + 1.0 mM EGTA
- **4′**: 35 nM QD-3MPA + 1.5 mM Ca^{2+} + 1.5 mM EGTA
- **5′**: 35 nM QD-3MPA + 2.0 mM Ca^{2+} + 2.0 mM EGTA
- **6′**: 35 nM QD-3MPA + 2.5 mM Ca^{2+} + 2.5 mM EGTA

Agarose Gel Electrophoresis. Agarose gel electrophoresis was performed as elsewhere,[4,23] except ethylenediamine tetraacetic acid (EDTA) was omitted from our gel buffer solution because EDTA binds Ca^{2+}. The gel buffer solution thus contained 40 mM Tris base and 20 mM acetic acid and had a pH value of 8.2 (later, we used HCl and NaOH to modify the pH value of the gel buffer solution to study the acid dissociation of 3MPA ligands on QDs).

The agarose gel concentration was 1.5%, and was run at 60 V for 5 h, with short interruptions for taking photos under a UV table using a common CCD digital camera equipped with a UV lens filter. We also recorded the photos by using the 600 channel with a diffuse light source at 520 nm of a Dual-Mode Imaging System Odyssey Fc (LI-COR). Both recording methods gave exactly the same results. The QD fluorescence signal was presented as red in the photos. Moreover, we calibrated the voltage distribution in the gel box. At 60 V, the electric field was found to be uniform and the value was 3.89 V/cm, and at 40 V, it was 2.57 V/cm, i.e., 3.89:2.57 ≈ 60:40, showing that the electric field in the gel box was linear. Similar bias and time duration (100 V for 1.5 h) were used for amino QDs,[4] while Pons et al. applied an electric field of 30 V/cm for 20 s followed by 15 V/cm for 15 min.[23]

The loading of the QD samples on the gel was performed in two different ways: (1) 100 μL QD samples were first loaded into the loading wells, then covered with 70 μL gel. Electrophoresis was run 10 min later after the covering gel had become hardened. Note that the volumes of the loaded QD samples were very large when compared with our early work[4] (100 vs 1 μL). Such large loading volumes were required in order to visualize the QD fluorescence signals from QD samples with a QD concentration of only 35 nM (which was due to the up-limits of the biologically relevant concentrations of Ca^{2+} and EGTA[15]). (2) QD samples were first mixed with a loading buffer (60% glycerol in HEPES) at a ratio of 5:1 and then loaded into the loading wells. Glycerol makes the sample buffer denser than the surrounding buffer of the gel, thus enabling easy sample loading into the wells and reducing the diffusion of the samples out of the wells.

QD Fluorescence Lifetime Measurement. We performed time-resolved fluorescence measurements of our QDs in the following manner using a time-correlated single-photon counting machine (FluoroMax-3, Horiba Jobin Yvon). A spectral line centered at 495 nm with a 2 nm bandpass from a pulsed light-emitting diode (peak wavelength 495 and 30 nm

fwhm) was led to the cuvette containing the QD aqueous solution in the form of a train of pulses (pulse duration was ca. 1.4 ns) at 1 MHz. The detector was set at the QD fluorescence peak wavelength with a bandpass of 2 nm. There were 2048 TAC channels with a variable integration time δ ranging from 50 ns to 1 μs. The photon counting was stopped when the maximal number of photon counts of the TAC channels reached a preset maximal photon-count value N_{max}. δ and N_{max} were adjusted in order to reach a high signal-to-noise ratio.

■ **RESULTS AND DISCUSSIONS**

Acid Dissociation of 3-MPA Ligands on QD. The carboxylic group of 3MPA was shown to be largely acid dissociated for pH values higher than 5 by Raman spectral study.[30] pK_a = 4.34 is given in a book from 2008.[31] It was reported in 2008 that the apparent surface pK_a of 3MPA on gold varied.[32] No report so far has been published about pK_a of 3MPA ligands on colloidal QDs. The equilibrium of the acid dissociation can be written as in standard textbook format
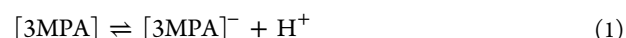
$$[3MPA] \rightleftharpoons [3MPA]^- + H^+ \tag{1}$$

where [3MPA]$^-$ denotes the dissociated 3MPA. Since the concentration of H$^+$ is determined by the pH value of the QD solution, i.e., pH = $-\log_{10}[H^+]$, the ratio between dissociated and undissociated 3MPA ligands is

$$\beta = \frac{[3MPA]^-}{[3MPA]} = 10^{pH-pK_a} \tag{2}$$

For pH = 7.34 and pK_a = 4.34, β = 10^3, meaning that 3MPA ligands are largely dissociated.[33] The dissociation of 3MPA ligands on the QD surface was qualitatively confirmed by the electrophoresis where our QD-3MPA migrated toward the anode and was thus negatively charged. The quantification of the dissociation of 3MPA ligands on the QD surface is, however, very complicated.

It was reported that the number of surface ligands per nm^2 on the surface of one QD ranges from 1 to 5[34] based on which we expected about 88 to 440 surface ligands per QD for our QDs of 5.6 nm in diameter. On the other hand, it is easy to estimate the maximal surface density of 3MPA ligands, which is about one 3MPA ligand per two Zn atoms, when the long axis of the 3MPA ligands is positioned normal to the QD surface. For our QD of approximately 5.6 nm in diameter, the number of surface Zn atoms is about 1000,[35] indicating that the number of 3MPA ligands per QD is 500, which agrees well with the above value of 440. The picture of all these 3MPA ligands per one QD being dissociated is not very realistic mostly due to the implicated huge electrostatic repulsion among terminal carboxylates of so many deprotonated 3MPA ligands on one QD of only 5 nm in diameter.

To quantify the degree of acid dissociation of 3MPA ligands on the QD surface, we performed electrophoresis of our QD-3MPA at different pH values of the gel buffer solution and the result is presented in Figure 2. We were aware of pK_a = 8.06 for Tris base and 4.8 for acetic acid so that the results of pH = 7.2, 6, and 5 in Figure 2 might not reflect the true electrophoretic mobilities of our QDs at these pH values. The extrapolation from pH = 9 and 8.2 to low pH values, i.e., the dashed line in Figure 2, shows that when the pH value of the gel buffer solution is larger than a certain value between 6 and 7, our QDs started to migrate toward the anode, indicating the beginning of the detectable acid dissociation. It was therefore concluded that
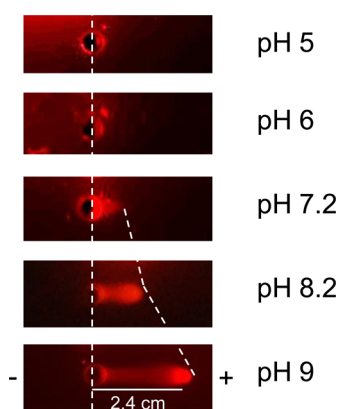
Figure 2. Electrophoresis of 3MPA-coated QDs at different pH values. The voltage was 60 V and the gel was run for 60 min.

the degree of the acid dissociation is strongly pH-dependent, resulting in a pH-dependent electrophoretic mobility when pH > 7.

Note that the fluorescence of QDs was extremely weak after 1 h of electrophoresis when the pH value of the gel buffer solution was below 7. The brightness of photos of pH = 5 and 6 in Figure 2 was therefore enhanced in order to visualize the positions of the loading wells. The decrease of the QD fluorescence in the gel buffer solution was expected due to interactions between QDs and ions, see more discussions below.

In order to understand Figure 2 in terms of pK_a = 4.34 of free 3MPA,[31] we measured the fluorescence intensity and decay spectra of QD-3MPA solutions at different pH values. The results are presented in Figures 1b and 3, showing that at pH
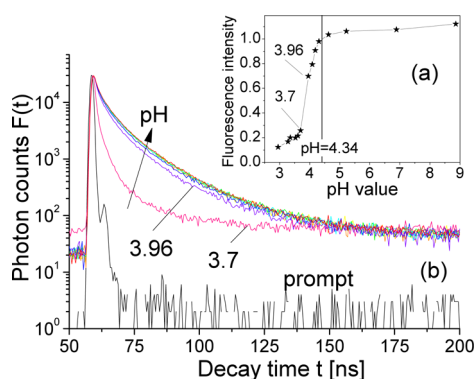

Figure 3. Fluorescence properties of QDs as functions of the pH value of the QD solution. Fluorescence spectra of QDs in solutions of different pH values are shown in Figure 1b. (a) Integrated fluorescence intensity vs pH value of the QD solution. (b) Time-resolved fluorescence decay spectra of QDs. The arrow marks the pH increase from 3.7, 3.96, 4.19, 4.31, 5.22, and 6.89 to 8.86. δ = 0.4950604 ns and N_{max} = 30000. The energy relaxation time τ was fitted to be ca. 2.0 ns and the radiative recombination time β ca. 8.1 ns for pH values ranging from 8.86 to 3.93.

value above pK_a of free 3MPA ligands, the florescence intensity increased following the increase of pH value while the fluorescence decay spectrum was insensitive to the pH variation. For pH < pK_a, both the fluorescence intensity and lifetime drastically decreased. Using the analysis method of ref.,[26] it was obtained that the energy relaxation time τ was ca. 2.0 ns and the radiative recombination time β ca. 8.1 ns for pH

values ranging from 8.86 to 3.93. We further noticed a small red shift in the QD fluorescence peak at low pH values in Figure 1b as mentioned before.

To understand the drastic change in both the fluorescence intensity and the fluorescence decay spectra when the pH value was decreased below 4, we studied the QD solution using confocal microscopic imaging. Here we found significant QD precipitations at low pH values. Figure 4a shows the QD
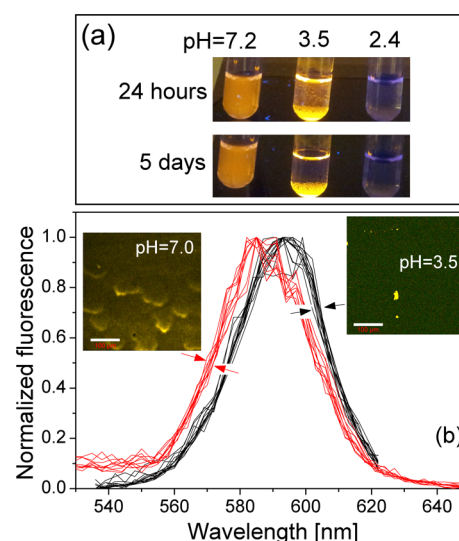

Figure 4. Precipitation of QDs at low pH values. (a) QD solutions of different pH values on a UV table. (b) Fluorescence spectra of QD deposits on microscope slides. Insets are confocal Lambda mode images.

solutions (QD concentration ca. 200 nM) on a UV table 1 day and 5 days after pH value modification, where we observed clearly the QD precipitation at pH = 3.5. Note the samples were kept still at 4 °C for the whole 5 days except when they were carefully placed on the UV table for photographing. The microscopic process was now unraveled: At pH = 2.4, the fluorescence was reduced directly after the pH modification. Nothing happened immediately after the pH value was modified from 7.2 to 3.5. However, 1 day later, QDs at pH = 3.5 began to form clusters then precipitated due to gravity. We deposited one drop of the QD solution into a circular area formed by nail polish on a microscope slide then covered it by a coverslip. Fluorescence emissions from QDs deposited on the microscope slides were excited by a 405 nm excitation laser using a confocal microscope (Zeiss LSM 780) with a Plan-Apochromat 20 × /0.8 objective (Carl Zeiss) and recorded with a spectral resolution of 2.9 nm. The image frame size was 423 × 423 μm^2 (pixel size 1.66 × 1.66 μm^2). Software ImageJ was used to obtain the fluorescence spectra of QDs from randomly chosen fluorescent spots (3 × 3 pixels), which were normalized by their peak fluorescent intensities and presented in Figure 4b. Here the correlation between the QD precipitation and fluorescence spectrum was clearly demonstrated. And the red-shift of the fluorescence peak was reconfirmed, which was principally due to the quantum size effect (large QDs emit at long wavelength). A large QD size implies a reduced quantum confinement so that the radiative recombination of the exciton inside the QD is reduced, resulting in the reduced fluorescence intensity,[36] which was reflected in both Figures 1b and 4b.

The drastic changes in Figure 3 when pH < 3.9 (see also the increased noise level of the lifetime curve of pH = 3.7 in Figure 3b) were the results of QD precipitation. Since aggregated QDs were shown to fluoresce less than dispersed QDs,[37] while the QD dispersion in water is mainly due to the electrostatic repulsion among QDs, we concluded that for pH below 4, 3MPA on the QD were undissociated so that QD-3MPA was not charged, leading to the observed QD precipitations and thereafter the drastic fluorescence and lifetime reductions.

Figure 3 indicates that when the pH value of the QD solution was higher than pK_a of the free 3MPA ligands, 3MPA-coated QDs started acid dissociation. The impart of pH-dependent pK_a of surface ligands to QDs was reported for cysteamine capped CdTeSe−ZnS core−shell QDs.[19] Above pK_a, the acid dissociation degree of 3MPA on the QD surface increased following the increase of the pH value, resulting in the increased QD fluorescence intensity due to less precipitation. Because of the large number of 3MPA ligands on the QD surface and the dynamic nature of the acid dissociation and association, we can envisage a spherical H$^+$ cloud surrounding acid dissociated QD-3MPA, see Figure 5. Acid dissociation
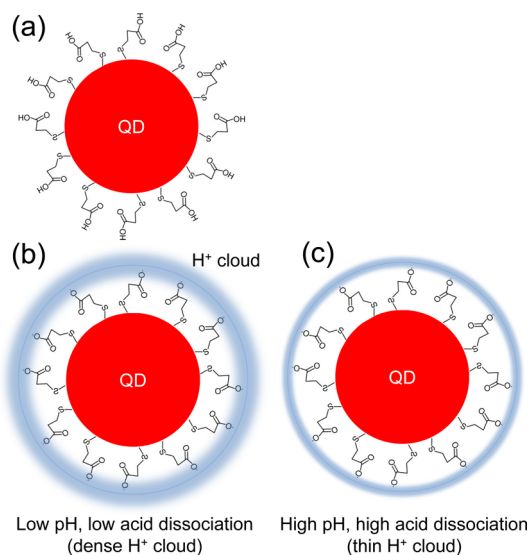

Figure 5. Acid dissociation of 3MPA ligands on the QD surface. (a) Schematic structure of 3MPA ligands on the QD surface. (b) Protons are represented by the H$^+$ cloud. Acid dissociation degree is low at low pH, resulting in a dense H$^+$ cloud. (c) High acid dissociation (thin H$^+$ cloud) at high pH values.

degree is low at low pH, resulting in a dense H$^+$ cloud; At high pH, the acid dissociation is increased and the H$^+$ cloud becomes thin. Using the quantum mechanical picture of QD exciton states of ref.,[26] it was easy to understand that because of the spherical symmetric distribution of the H$^+$ cloud on the QD surface, the degree of 3MPA acid dissociation on the QD surface would not affect the exciton states inside the QD, making the fluorescence decay of the QD largely pH-independent, as shown in Figure 3b.

In order to understand the limited electrophoretic mobility of QDs at pH below 7 in Figure 2, we followed the general theoretical framework of Strating and Wiegel[38] to calculate electric screening effect on a charged QD exerted by its surrounding counterions in the gel buffer solution. We consider a spherical QD so we work in the spherical coordinate system to utilize the spherical symmetry of our system. Let the QD sit

at the origin of the spherical coordinate system. The radius of the QD is R and the QD is charged with $-Qe$, where e is the unit charge. We consider two types of counterions in the gel buffer solution whose concentrations are denoted as $\rho_1(r)$ positively charged with e and $\rho_2(r)$ negatively charged with $-e$ (only one type of counterions was considered in ref 38). The local current density of counterions is given by

$$j_1 = -D_1 \frac{d\rho_1}{dr} - e\rho_1\mu_1\frac{d\phi}{dr}, \quad j_2 = -D_2\frac{d\rho_2}{dr} + e\rho_2\mu_2\frac{d\phi}{dr}$$

(3)

where D_1 and D_2 are diffusion coefficients and μ_1 and μ_2 are mobilities, which are related by the Einstein relation $D/\mu = k_BT$, where k_B is the Boltzmann's constant and T the temperature. ϕ is the electric potential determined by the Poisson equation

$$\frac{1}{r^2}\frac{d}{dr}\left(r^2\frac{d\phi}{dr}\right) = -\frac{e(\rho_1 - \rho_2)}{\epsilon}$$

(4)

for $r > R$. At thermal equilibrium, $j_1 = j_2 = 0$ so that

$$\frac{1}{\rho_1}\frac{d\rho_1}{dr} = -\frac{e}{k_BT}\frac{d\phi}{dr}, \quad \frac{1}{\rho_2}\frac{d\rho_2}{dr} = \frac{e}{k_BT}\frac{d\phi}{dr}$$

(5)

Numerical results of $\phi(r)$, $\rho_1(r)$ and $\rho_2(r)$ are shown in Figure 6. Here $\epsilon = \epsilon_r\epsilon_0$, $\epsilon_r = 80$ for water at room temperature.
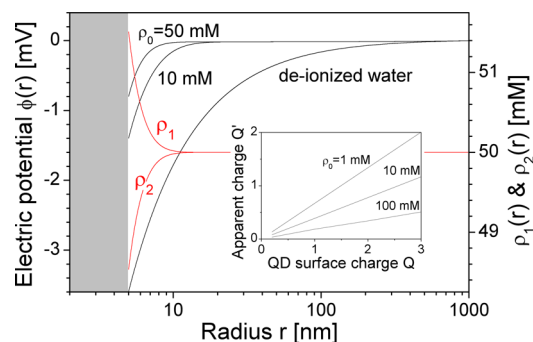

Figure 6. Screening effect of the QD surface charge (QD radius $R = 5$ nm, i.e., shadow area, and $Q = -1$) by ions in the QD solution. Left vertical axis (black lines): electric potential $\phi(r)$ as a function of radius r when the QD is in deionized water ($\rho_0 = 0$) and in a solution medium of different ion concentration ($\rho_0 = 10$ and 50 mM). Right vertical axis (red lines): ion distributions $\rho_1(r)$ and $\rho_2(r)$ for $\rho_0 = 50$ mM. Inset: apparent charge Q' (QD surface charge plus screening charges) vs QD surface charge Q in QD solution medium with different ion concentration $\rho_0 = 1$, 10, and 100 mM. $T = 300$ K.

$|\rho_1(\infty)| = |\rho_2(\infty)| = \rho_0$. Near the QD surface, ρ_1 was much increased due to Coulomb attraction while ρ_2 was decreased, resulting in the expected screening effect. As previously indicated, our gel buffer solution contained 40 mM Tris base and 20 mM acetic acid and the pH value was modified by adding HCl or NaOH, for which we expected ρ_0 to be in the order of 50 mM. For $\rho_0 = 50$ mM, ϕ is only -0.8 mV at the QD surface. By comparing with $\phi = -3.6$ mV for $\rho_0 = 0$, it was concluded that the QD was strongly screened, which was quantified by introducing a parameter called the apparent charge $-Q'$ defined by

$$\phi(r)|_{r=R} = \frac{-Q'}{4\pi\epsilon R}$$

(6)

whose numerical results were shown in the inset in Figure 6. The small electrophoretic mobility of QDs at pH below 7 was thus the result of the electric screening of the QD surface charge by ions of high concentrations in the gel buffer solution.

Electrophoretic Mobility of QD-3MPA vs Ca^{2+} and EGTA. Figure 7 displays the photos of the QD samples at

(a) QDs without/with Ca^{2+} (covered with gel)

1 2 3 4 5 6

0 h   1 h   2 h   3 h   4 h

(b) QDs without/with Ca^{2+}+EGTA (covered with gel)
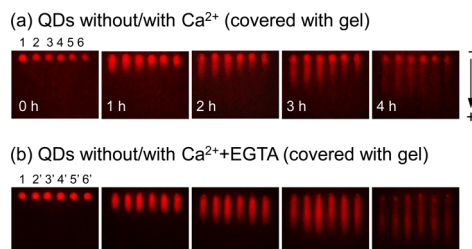
1 2' 3' 4' 5' 6'

Figure 7. Agarose gel (1.5%) electrophoresis of QD-3MPA at 60 V (3.89 V/cm). 35-nM QD samples were first loaded then covered by gel. pH = 8.2. (a) QDs in the absence and presence of Ca^{2+}. Sample **1**: pure QDs. Samples **2**, **3**, **4**, **5**, and **6**: 35-nM QDs plus 0.5, 1.0, 1.5, 2.0, and 2.5 mM Ca^{2+}. (b) QDs in the absence and presence of Ca^{2+} and EGTA. Samples **2'**, **3'**, **4'**, **5'**, and **6'**: 35-nM QDs plus 0.5, 1.0, 1.5, 2.0, and 2.5 mM Ca^{2+} and EGTA.

various times of electrophoresis. QD-3MPA (sample **1**) moved toward the anode, indicating that these QDs were acid dissociated and thus negatively charged. We observed here that the migration of the acid dissociated QD-3MPA under the electric field was slowed down by Ca^{2+} (samples **2**, **3**, **4**, **5**, and **6** of 35-nM QDs with 0.5, 1.0, 1.5, 2.0, and 2.5 mM Ca^{2+}, respectively), see Figure 7(a), and the further addition of EGTA (samples **2'**, **3'**, **4'**, **5'**, and **6'** of 35-nM QDs with 0.5, 1.0, 1.5, 2.0, and 2.5 mM Ca^{2+} and EGTA, respectively) restored the electrophoretic mobility of QD-3MPA toward the anode, see Figure 7b. Most importantly, Figure 7a shows that the electrophoretic mobility of QD-3MPA was maximally diminished in the presence of more than 2.0-mM Ca^{2+} (sample **6**), which was exactly the same Ca^{2+} concentration required to maximally quench the fluorescence of 35-nM QDs, see Figure 1c. Note that the electrophoresis was run continuously for more than 4 h. This indicates clearly that the interaction between Ca^{2+} and dissociated QD-3MPA is very strong, resulting in QD-3MPA−Ca^{2+} being a stable charge-neutral complex when the concentration of Ca^{2+} ions reached 2.5 mM for 35-nM QDs. Otherwise, such as in the situation of collisional interaction, dissociated QD-3MPA and Ca^{2+} were gradually separated in space by the electric field so that we would not observe the clean and persistent decrease of the electrophoretic mobility of QD-3MPA in the presence of Ca^{2+} ions.

We noticed the stretched tails in all columns. To understand it, we loaded QD samples in a different way. Figure 8 shows the photos of the QD samples on UV light, where the QD samples were first mixed with glycerol and then loaded. Exactly the same phenomena regarding the electrophoretic mobility of the QDs were observed here as in Figure 7, while the loading wells were now devoid of QDs after applying the voltage. This suggests that covering loading wells with gel caused retention of QDs in the loading wells and the high gel concentration of 1.5% may be the reason for the persistent QD tails in Figures 7 and 8.

Another possible cause of the QD tails is a distribution of different species in a given reaction mixture such as
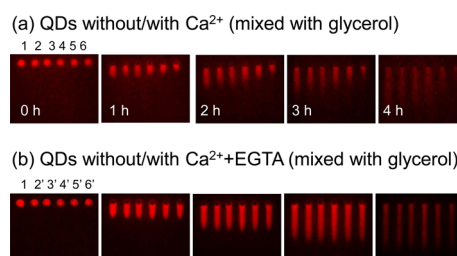

(a) QDs without/with Ca^{2+} (mixed with glycerol)

1 2 3 4 5 6

0 h   1 h   2 h   3 h   4 h

(b) QDs without/with Ca^{2+}+EGTA (mixed with glycerol)

1 2' 3' 4' 5' 6'

Figure 8. Same as Figure 7 but the QD samples were first mixed with glycerol then loaded.

undissociated and dissociated QD-3MPA, QD-3MPA−Ca^{2+} complex, as well as the dynamic processes of acid dissociation and interactions among species. To clarify this, we reduced the gel concentration to 0.5% and found that the tail was significantly reduced, see Figure 9a. It is thus concluded that
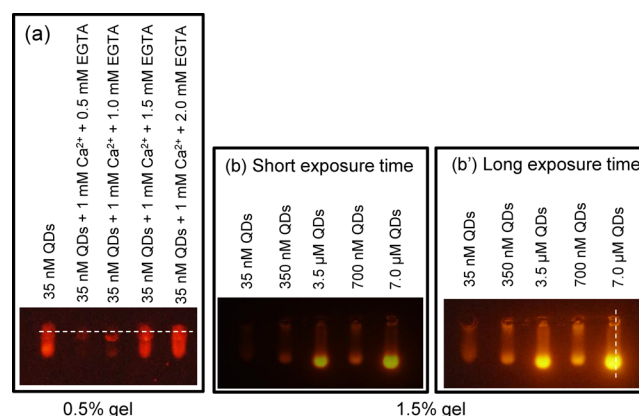

Figure 9. (a) Agarose gel (0.5%) electrophoresis at 30 V for 1 h. QD samples were first loaded then covered by gel. The horizontal dashed line marks the positions of the loading wells. (b) Agarose gel (1.5%) electrophoresis at 60 V for 1 h for different QD concentrations. (b') Same as part b but after a long exposure time that revealed the QD tails.

a small amount of QDs get stuck in the gel matrix during electrophoresis. We restored the gel concentration to 1.5% while increased the QD concentration to a few μM, as used in most electrophoresis experiments.[4,23] The results are shown in Figure 9, parts b and b'. It is observed here that the QD tails were no longer visible when the fluorescence signal from highly concentrated QDs was recorded by auto exposure mode, while the tails became visible when the exposure time was prolonged, and the intensities of the tails were more or less the same for different QD concentrations (35 nm, 350 nM, 700 nM, 3.5 μM and 7.0 μM studied here), see Figure 9b'. We thus showed that the persistent QD tails in Figures 7 and 8 were largely caused by the retention of QDs in the gel.

The weak dependence of the tails on the QD concentration in Figure 9b' also ruled out the possibilities of significant QD size effect and/or nonhomogeneous 3-MPA coating on the QD surface since they would imply a tail which is proportional to the QD concentration.

Figures 7, 8 and 9 demonstrate that there was a strong interaction between the dissociated QD-3MPA and Ca^{2+} which resulted in the stable charge-neutral QD-3MPA−Ca^{2+} complex and that the fluorescence and electrophoretic mobility of the dissociated QD-3MPA were largely quenched by the closely

attached Ca^{2+}, which were revived by adding EGTA that chelated the Ca^{2+} ion away from the dissociated QD-3MPA.

We also studied the electrophoretic mobility of our QDs when only EGTA (1.0 mM) was added to the QD solutions and found out that EGTA did not change QDs' electrophoretic mobility (it did, however, modify QDs' fluorescence intensity, see also ref.[15]). This is consistent with the fact that EDTA, which is similar to EGTA normally present in the buffer solution of electrophoresis, did not affect the QDs' electrophoretic mobility.[4,23]

Fluorescence lifetime spectra of QD-3MPA solutions in the presence of different Ca^{2+} concentrations are presented in Figure 10a. By using the quantum mechanical model of exciton
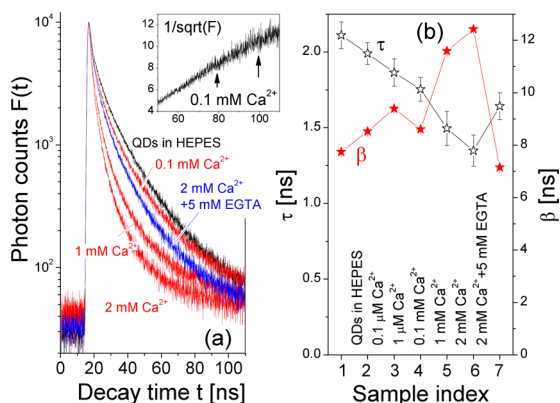

Figure 10. (a) Time-resolved fluorescence spectrum $F(t)$ of QDs under the influence of Ca^{2+} and EGTA. Inset shows $1/\sqrt{F}$ when the Ca^{2+} concentration was 0.1 mM. $\delta = 0.05746$ ns and $N_{max} = 10000$. (b) Energy relaxation time τ and radiative recombination time β.

states in the QD of ref [26], we obtained the relaxation time τ of photoexcited exciton to the exciton ground state and the exciton radiative recombination time β as functions of Ca^{2+} concentration presented in Figure 10b. It was clearly observed that the exciton relaxation time τ was inversely proportional to the Ca^{2+} concentration, while exciton radiative recombination time β increased following the increase of the Ca^{2+} concentration. This was very different from the fluorescence decay spectra of different pH values shown in Figure 3, where the fluorescence decay spectrum remained largely unchanged when the pH value of the QD solution was modified (for pH > 4). Note that β of the QD sample with 0.1 mM Ca^{2+} ions was abnormal due to measurement errors marked by vertical arrows in the inset of Figure 10a (which is hardly perceptible in $F(t)$ itself).

The different behaviors of the fluorescence decay data fit the microscopic picture of the exciton states in the QD. At pH > 4 QDs remained largely single in the QD solution. The acid association of 3MPA ligands on the QD surface is spherical (see Figure 5) so that the wave functions of electron and hole states inside the QD remained spherical, independent of the degree of the acid association. τ and β were therefore largely pH-independent. On the other hand, an association of one Ca^{2+} ion on the QD surface attracts the electron and repels the hole so that the radiative recombination time β between the electron and the hole is increased. Meanwhile, energy relaxation time τ of the photoexcited exciton was decreased by the Ca^{2+} association since the electron and hole wave functions were edging toward the QD surface so were more accessible to

surface states which increased the energy relaxation process (thus a reduced energy relaxation time).

Optical Spectrum of QDs during Electrophoresis. While the decrease of the QD fluorescence intensity due to the addition of Ca^{2+} was not very clearly delineated in the photos of electrophoresis, mostly due to the auto exposure mode of the camera, see Figures 7a and 8a, it was nevertheless present in the fluorescence spectra of these QD samples, see Figure 1c.

The fluorescence of QDs was greatly affected by the agarose gel electrophoresis. As shown in Figures 7 and 8, the fluorescence intensity became weak along the course of electrophoresis. One obvious factor was the tail and diffusion of QDs in the gel matrix. We used a Thorlabs CCS100 spectrometer and a laser of 402 nm (laser spot size ca. 1 mm in diameter) to measure the fluorescence spectrum of QDs along the vertical line shown in Figure 9b′, see the schematic setup in Figure 11a. The spectrum as a function of the z position is
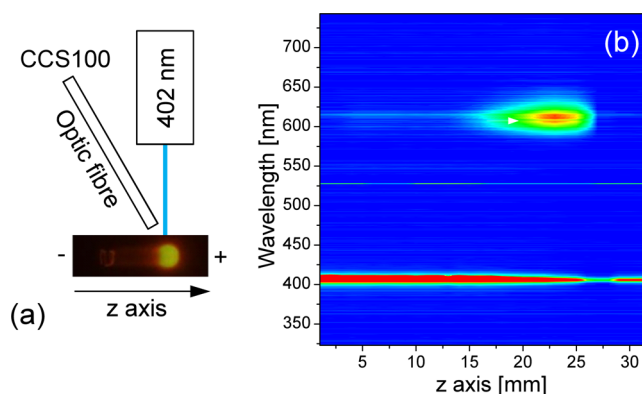

Figure 11. (a) Setup to measure the fluorescence spectrum (b) of QD612 distributed along the electrophoretic migration path of QDs.

presented in Figure 11b showing the migration and diffusion of QDs. The fluorescence peak wavelength of QDs remained unchanged during electrophoresis. Note that a dip at 603 nm existed in all the spectra which was caused by a black pixel in our spectrometer.

Discussions and Theoretical Studies of Acid Dissociation of QD-3MPA and Interaction with Ca^{2+}. Our QDs consisted of CdSe cores and $CdS/Cd_{0.5}Zn_{0.5}S/ZnS$ multishells. The materials, CdS and ZnS, used for the multishell structure, have larger energy bandgaps than that of CdSe so that the wave functions of the photoexcited electron and hole are largely confined to the CdSe core region, the radiative recombination of the electron and hole is thus protected from many nonradiative factors outside of the CdSe core. However, the large energy bandgaps of CdS and ZnS are still finite so that the wave functions of the electron and hole will unavoidably penetrate the multishell structure to reach QD's surface and environment.[28]

When a positively charged Ca^{2+} ion binds the QD surface, it generates a long-range electrostatic potential to attract the wave function of the electron and repel the wave function of the hole. The effects are 2-fold. First of all, the wave functions of the electron and the hole are separated in space so that their radiative recombination is reduced, resulting in a reduced fluorescence intensity and a longer radiative recombination lifetime β in Figure 10b. Second, as the spatial distributions of the wave functions of the electron and the hole are now shifted

toward the QD surface, surface states of the QD and QD's dielectric medium affect more strongly the electron and the hole and thereafter QD's fluorescence properties, resulting in a faster energy relaxation process τ shown Figure 10b.

To understand the physical and chemical nature about 3MPA on the QD surface and the interaction between QD-3MPA and Ca^{2+} based on our experimental results, we performed first-principles studies. All geometries were fully optimized through the hybrid exchange-correlation functional B3LYP[39−42] in combination with all-electron split valence 6-31G(d) basis set for nonmetal atoms[43] and LANL2DZ for transition metal ions. Vibrational analyses were conducted at the same level. Solvent effects were included by using the conductor-like polarizable continuum model (CPCM)[44,45] with the molecular cavity defined by UAKS radii. The calculations were carried out with Gaussian 09 program.[46] A Zn_6S_6–3MPA cluster was chosen to model our QD-3MPA.[27] The proton affinity (ΔG) of the Zn_6S_6–3MPA cluster, computed by subtracting the energies of the proton (H^+) and the dissociated $[Zn_6S_6$–3MPA$]^-$ cluster from the energy of the undissociated $H^+[Zn_6S_6$–3MPA$]^-$ cluster by the following equations

$$H^+ + [Zn_6S_6\text{–3MPA}]^- \rightleftharpoons H^+[Zn_6S_6\text{–3MPA}]^- \tag{7}$$
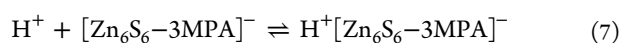
$$\Delta G = G_{H^+[Zn_6S_6\text{–3MPA}]^-} - G_{H^+} - G_{[Zn_6S_6\text{–3MPA}]^-} \tag{8}$$

is used to measure the acid strength of QD-3MPA. Here, G is the Gibbs free energy with thermal correction at 298.15 K. The calculated proton affinity ΔG for the Zn_6S_6–3MPA cluster was −13.171 eV in gas phase and −8.387 eV in water. This clearly indicated the ability of the Zn_6S_6–3MPA cluster to acid dissociate in water, which agrees quantitatively with the experimental observation that our QD-3MPA in water was negatively charged.

By including the solvent effects, the computed interaction between undissociated Zn_6S_6–3MPA cluster and Ca^{2+} was 5.477 eV in gas phase and 0.497 eV in water, and the computed interaction between dissociated Zn_6S_6–3MPA and Ca^{2+} was 12.411 eV in gas phase and 1.048 eV in water, respectively. Here we first observed a large reduction in the interaction in water which is mainly due to the screening effect caused by the polar water molecules. Figure 12 shows the optimized structures of undissociated and dissociated Zn_6S_6–3MPA cluster and Ca^{2+} in water. Our calculations thus show that

dissociated Zn_6S_6–3MPA interacted more strongly with Ca^{2+} owing to the ionic nature of the interaction.

To address the binding of multiple 3MPA ligands to the external ZnS surface of our QD, we chose the (0001) surface of ZnS and performed first-principles simulation with Perdew−Burke−Ernzerhof generalized gradient approximation exchange and correlation functionals[47] using plane-wave basis sets implemented in Vienna ab initio simulation package (VASP).[48−50] A cutoff dynamic energy of 400 eV was used, and the nuclei and core electrons of the atoms were described using projector augmented-wave (PAW) potentials.[51,52] For interactions over the Brillouin zone, we used a 5 × 5 × 1 Monkhorst−Pack grid.[53] A 4 × 2 supercell was employed. A slab model of ZnS (0001) surfaces with 4 atomic layers was considered (totally 32 atoms), with a 10 Å vacuum region between two successive slabs. The positions of the atoms in the two bottom layers were fixed, while the spatial positions of other atoms were allowed to be relaxed. Note that the current VASP study did not include solvent effects.

As discussed above, there were two 3-MPA ligands in our slab model, i.e., one 3MPA ligand for every two Zn atoms at the QD surface. To find the optical geometrical positions of the two 3MPA ligands on the ZnS surface, we calculated the total energy as a function of the spatial separation between the two 3MPA ligands. Four alternatives were studied, namely, 3.812, 4.938, 7.650, and 8.752 Å, on the ZnS (0001) surface and it was found that the most energetically favored structure was the one when the two 3MPA ligands were separated initially by 7.650 Å, see Figure 13.

Figure 13. Optimized structure of two 3MPA ligands periodically positioned on the ZnS (0001) surface.

(a) Acid-undissociated cluster + Ca^{2+} in water with a binding energy 0.497 eV

2.99 Å
2.44 Å

(b) Acid-dissociated cluster + Ca^{2+} in water with a binding energy 1.048 eV
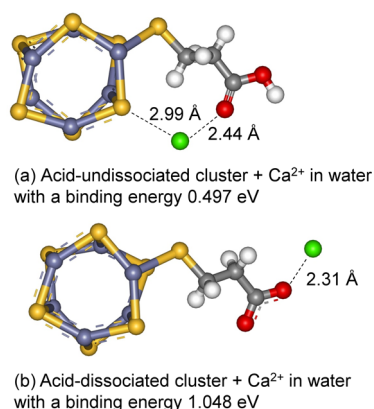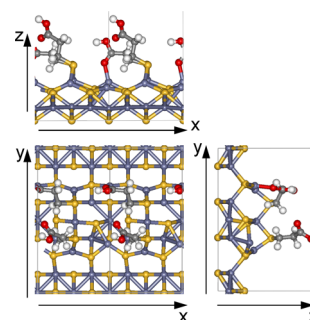
2.31 Å

Figure 12. Optimized structures of acid undissociated (a) and dissociated (b) ZnS−3MPA interacting with one Ca^{2+} ion. The Ca atom is in green, Zn in pale blue, S in yellow, O in red, C in gray, and H in white.

We notice that in Figure 13, the 3MPA ligands attach to the QD surface at tilted angles so that one oxygen atom of the carboxyl group (not the oxygen atom at the hydroxyl terminal) interacts with the ZnS surface (most clearly in the xz side view). This coupling results in a tighter packing of the carboxyl group toward the ZnS surface. Such a geometrical steric effect will hinder the O−H bond dissociation, i.e., the acid dissociation of the 3MPA ligand, which may be the very reason for the limited degree of acid dissociation of QD-3MPA at pH value below 7 shown in Figure 2. With an increase of the pH value, the increased concentration of the hydroxide molecules in the QD solution is expected to disrupt the interaction between the carboxyl group of the 3MPA ligand and the QD surface. This, in turn, forces the carboxyl group of the 3MPA molecule to extend into the solution, thus increasing the acid dissociation, and therefore the charge per QD as the pH value increases.

We subsequently positioned one Ca^{2+} ion initially at the terminal regions of the two acid dissociated 3MPA ligands to study its interaction with the carboxyl groups of the two ligands via electrostatic interactions. Moreover, we also investigated another binding possibility, namely, Ca^{2+} ion close to the ZnS surface with couplings to both the S atoms of the 3MPA ligands and the ZnS surface. The optimized structures of the two approaches are presented in Figure 14. Two small horizontal
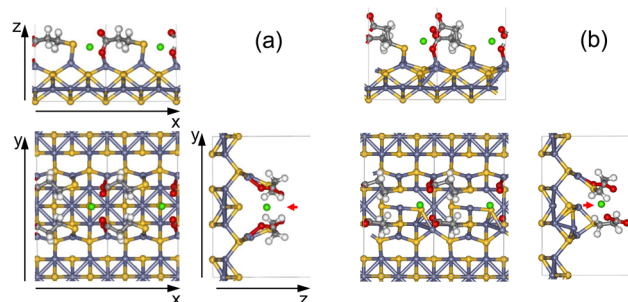

Figure 14. Optimized structures of two dissociated ZnS−3MPA ligands with one Ca^{2+} ion. (a) The initial position of the Ca^{2+} was at the terminal regions of the dissociated 3MPA ligands. (b) The Ca^{2+} ion was initially positioned close to the ZnS surface. The two small horizontal arrows in the yz side views mark the trajectories of the Ca^{2+} ions during structure optimizations.

arrows in the yz side views mark the trajectories of the Ca^{2+} ions during structure optimizations. The binding energy of the first approach was 9.841 eV, it was 6.951 eV for the second approach. The reason for the difference in the interaction energies can be well understood by analyzing the optimized structures.

In the first binding approach of Figure 14a, Ca^{2+} interacts almost equally with the two ligands. Because of the negative charges in the terminal regions of the ligands, one of the oxygen atom in the carboxyl group of one ligand interacts with the ZnS surface by forming an O−Zn bond of 1.96 Å. The other oxygen in the carboxyl group interacts with Ca^{2+} ion at a distance of 2.52 Å to one ligand and 2.42 Å to the other ligand. Furthermore, Ca^{2+} interacts with two S atoms of the 3MPA ligands at a distance of 3.00 Å, in addition to the interaction with the surface S atom at a distance of 3.03 Å.

In the second binding approach of Figure 14b, the oxygen atom in the carboxyl group of one ligand interacts with Ca^{2+} very tightly at a distance of 2.09 Å, which hinders the interaction between the other oxygen atom in the same carboxyl group and the Zn ion of the ZnS surface. The two oxygen atoms in the other ligand interact with Ca^{2+} at the distances similar to that in Figure 14a. In addition, the two S atoms in the ligands interact with Ca^{2+} with the shortest distance of 3.20 Å which is considerably longer than that in Figure 14(a).

The conformations of Figure 14, parts a and b, are rather alike in general, all showing that the paired dissociated 3MPA ligands on the QD surface associate tightly with one Ca^{2+} via strong Coulombic interactions. This was already shown experimentally, i.e., the modifications in the electrophoretic mobility and optical properties of 3MPA-coated QDs without Ca^{2+} ions and in the presence of Ca^{2+} ions. Most interestingly, the two conformations of Figure 14, parts a and b, show a remarkable resemblance to the one of the EGTA that chelates much strongly Ca^{2+}.

CONCLUSION

In a brief summary, we carefully devised electrophoresis and optical characterization experiments as qualitative indications of acid dissociation of mercaptoproionic acid coated CdSe−CdS/ $Cd_{0.5}Zn_{0.5}S$/ZnS core−multishell quantum dots (3-MPA-coated QDs) and developed a clear understanding of the nature of the 3MPA on the QD surface and interactions between 3MPA-coated QDs and Ca^{2+} ions in media with varying pH values. We probed changes in the electrophoretic mobility of the 3MPA-coated QDs when mixed with different concentrations of Ca^{2+} and further tested the effects of adding EGTA chelator to the mixture. It was found that, at pH below 7.0, the electrophoretic mobility of the 3MPA-coated QDs was very limited. When pH > 7.0, 3MPA-coated QDs were negatively charged due to the acid dissociation of the carboxyl group (acid-dissociated QDs) of 3MPA ligands on the QD surface. The acid-dissociated QD interacted strongly with Ca^{2+} ions, resulting in a stable charge neutral QD-3MPA−Ca^{2+} complex with a significantly reduced electrophoretic mobility. When EGTA was added to chelate Ca^{2+} and free the acid-dissociated QD-3MPA, the acid-dissociated QD-3MPA regained its original electrophoretic mobility. We applied first-principles calculations to understand our experimental results at microscopic level, unraveling the limited acid dissociation of 3MPA surface ligands on the QD surface in water and the strong ionic interaction between acid dissociated 3MPA-coated QD and Ca^{2+}. The insights obtained in this work can be very useful for developing QD-based microscopic biosensor.

Moreover, the strategy and techniques reported in this work are readily transferrable to other types of fluorescent biomarkers and therefore can be important for advancing QD applications in biological media such as in vivo and in vitro imaging, sensing and labeling.

AUTHOR INFORMATION

Corresponding Author
*(Y.F.) E-mail: fu@kth.se.

Author Contributions
N.S. and H.X. performed electrophoresis experiments, H.X. performed fluorescence decay measurements, H.X. and L.L. fabricated QDs, Y.Z. and J.W. performed first-principles calculations. All authors participated in the analysis, the discussion, and the development of the research work. All authors participated in the formulation and the review of the manuscript.

Notes
The authors declare no competing financial interests.

REFERENCES

(1) Sargent, E. H. Colloidal Quantum Dot Solar Cells. *Nat. Photonics* **2012**, 6, 133−135.
(2) Ning, Z.; Tian, H.; Yuan, C.; Fu, Y.; Qin, H.; Sun, L.; Ågren, H. Solar Cells Sensitized with Type-II ZnSe-CdS Core/Shell Colloidal Quantum Dots. *Chem. Commun.* **2011**, 47, 1536−1538.
(3) Zrazhevskiy, P.; Sena, M.; Gao, X. Designing Multifunctional Quantum Dots for Bioimaging, Detection, and Drug Delivery. *Chem. Soc. Rev.* **2010**, 39, 4326−4354.

(4) Chen, Y.; Molnár, M.; Li, L.; Friberg, P.; Gan, L.-M.; Brismar, H.; Fu, Y. Characterization of VCAM-1-Binding Peptide-Functionalized Quantum Dots for Molecular Imaging of Inflamed Endothelium. *PLoS One* **2013**, *8*, e83805.

(5) Lecavalier, M.-E.; Goulet, M.; Allen, C. N.; Beaulieu, L.; Lariviére, D. Water-Dispersible Colloidal Quantum Dots for the Detection of Ionizing Radiation. *Chem. Commun.* **2013**, *49*, 11629–11631.

(6) Banerjee, S.; Kar, S.; Santra, S. A Simple Strategy for Quantum Dot Assisted Selective Detection of Cadmium Ions. *Chem. Commun.* **2008**, 3037–3039.

(7) Chen, Y.; Rosenzweig, Z. Luminescent CdS Quantum Dots as Selective Ion Probes. *Anal. Chem.* **2002**, *74*, 5132–5138.

(8) Ruedas-Rama, M. J.; Hall, E. A. H. Azamacrocycle Activated Quantum Dot for Zinc Ion Detection. *Anal. Chem.* **2008**, *80*, 8260–8268.

(9) Zhang, Y.-H.; Zhang, H.-S.; Ma, M.; Guo, X.-F.; Wang, H. The Influence of Ligands on the Preparation and Optical Properties of Water-Soluble CdTe Quantum Dots. *Appl. Surf. Sci.* **2009**, *255*, 4747–4753.

(10) Callan, J. F.; McCaughan, B.; Mulrooney, R. C.; Kamila, S. Determination of Zinc in Aqueous Solution Using CdSe/ZnS Quantum Dots Functionalised with [Carboxymethyl-(4-Mercapto-Phenyl)-Amino]-Acetate. *Int. J. Biomed. Nanosci. Nanotechnol.* **2011**, *2*, 3–11.

(11) Chen, S.; Zhang, X.; Zhang, Q.; Hou, X.; Zhou, Q.; Yan, J.; Tan, W. CdSe Quantum Dots Decorated by Mercaptosuccinic Acid as Fluorescence Probe For Cu^{2+}. *J. Lumin.* **2011**, *131*, 947–951.

(12) Shang, Z. B.; Hu, S.; Wang, Y.; Jin, W. J. Interaction Of β-Cyclodextrin-Capped CdSe Quantum Dots with Inorganic Anions and Cations. *Luminescence* **2011**, *26*, 585–591.

(13) Molnár, M.; Ning, Z.-J.; Chen, Y.; Friberg, P.; Gan, L.-M.; Fu, Y. Effects of K^+ and Na^+ Ions on the Fluorescence of Colloidal CdSe/CdS and CdSe/ZnS Quantum Dots. *Sens. Actuators, B* **2011**, *155*, 823–830.

(14) Singh, N.; Mulrooney, R. C.; Kaur, N.; Callan, J. F. Fluorescent Recognition of Potassium and Calcium Ions Using Functionalised CdSe/ZnS Quantum Dots. *J. Fluoresc.* **2009**, *19*, 777–782.

(15) Li, L.; Chen, Y.; Tian, G.; Akpe, V.; Xu, H.; Gan, L.-M.; Skrtic, S.; Luo, Y.; Brismar, H.; Fu, Y. Reversible Modification of CdSe-CdS/ZnS Quantum Dot Fluorescence by Surrounding Ca^{2+} Ions. *J. Phys. Chem. C* **2014**, *118*, 10424–10433.

(16) Gao, X.; Chan, W. C. W.; Nie, S. Quantum-Dot Nanocrystals for Ultrasensitive Biological Labeling and Multicolor Optical Encoding. *J. Biomed. Opt.* **2002**, *7*, 532–537.

(17) Susha, A. S.; Javier, A. M.; Parak, W. J.; Rogach, A. L. Luminescent CdTe Nanocrystals as Ion Probes and pH Sensors in Aqueous Solutions. *Colloids Surf., A* **2006**, *281*, 40–43.

(18) Deng, Z.; Zhang, Y.; Yue, J.; Tang, F.; Wei, Q. Green and Orange CdTe Quantum Dots as Effective pH-Sensitive Fluorescent Probes for Dual Simultaneous and Independent Detection of Viruses. *J. Phys. Chem. B* **2007**, *111*, 12024–12031.

(19) Tang, R.; Lee, H.; Achilefu, S. Induction of pH Sensitivity on the Fluorescence Lifetime of Quantum Dots by NIR Fluorescent Dyes. *J. Am. Chem. Soc.* **2012**, *134*, 4545–4548.

(20) Ke, J.; Li, X.; Zhao, Q.; Hou, Y.; Chen, J. Ultrasensitive Quantum Dot Fluorescence Quenching Assay for Selective Detection of Mercury Ions in Drinking Water. *Sci. Rep.* **2014**, *4*, 5624.

(21) Jing, P. T.; Zheng, J. J.; Ikezawa, M.; Liu, X. Y.; Lv, S. Z.; Kong, X. G.; Zhao, J. L.; Masumoto, Y. Temperature-Dependent Photoluminescence of CdSe-Core CdS/CdZnS/ZnS-Multishell Quantum Dots. *J. Phys. Chem. C* **2009**, *113*, 13545–13550.

(22) Zhao, Y.; Riemersma, C.; Pietra, F.; Koole, R.; de Mello Donega, C.; Meijerink, A. High-Temperature Luminescence Quenching of Colloidal Quantum Dots. *ACS Nano* **2012**, *6*, 9058–9067.

(23) Pons, T.; Uyeda, H. T.; Medintz, I. L.; Mattoussi, H. Hydrodynamic Dimensions, Electrophoretic Mobility, and Stability of Hydrophilic Quantum Dots. *J. Phys. Chem. B* **2006**, *110*, 20308–20316.

(24) So, M. K.; Xu, C.; Loening, A. M.; Gambhir, S. S.; Rao, J. Self-Illuminating Quantum Dot Conjugates for in vivo Imaging. *Nat. Biotechnol.* **2006**, *24*, 339–342.

(25) Liu, W.; Howarth, M.; Greytak, A. B.; Zheng, Y.; Nocera, D. G.; Ting, A. Y.; Bawendi, M. G. Compact Biocompatible Quantum Dots Functionalized for Cellular Imaging. *J. Am. Chem. Soc.* **2008**, *130*, 1274–1284.

(26) Xu, H.; Chmyrov, V.; Widengren, J.; Brismar, H.; Fu, Y. Mechanisms of Fluorescence Decays of Colloidal CdSe-CdS/ZnS Quantum Dot Unraveled by Time-Resolved Fluorescence Measurement. *Phys. Chem. Chem. Phys.* **2015**, *17*, 27588–27595.

(27) Li, L.; Tian, G.; Luo, Y.; Brismar, H.; Fu, Y. Blinking, Flickering, and Correlation in Fluorescence of Single Colloidal CdSe Quantum Dots with Different Shells Under Different Excitations. *J. Phys. Chem. C* **2013**, *117*, 4844–4851.

(28) Ning, Z.; Tian, H.; Qin, H.; Zhang, Q.; Ågren, H.; Sun, L.; Fu, Y. Wave Function Engineering of CdSe-CdS Core-Shell Quantum Dots for Enhanced Electron Transfer to a TiO_2 Substrate. *J. Phys. Chem. C* **2010**, *114*, 15184–15189.

(29) Ning, Z.-J.; Molnár, M.; Chen, Y.; Friberg, P.; Gan, L.-M.; Ågren, H.; Fu, Y. Role of Surface Ligands in Optical Properties of Colloidal CdSe/CdS Quantum Dots. *Phys. Chem. Chem. Phys.* **2011**, *13*, 5848–5854.

(30) Castro, J. L.; López-Ramírez, M. R.; Arenas, J. F.; Otero, J. C. Surface-Enhanced Raman Scattering of 3-Mercaptopropionic Acid Adsorbed on a Colloidal Silver Surface. *J. Raman Spectrosc.* **2004**, *35*, 997–1000.

(31) *Electrochemical Sensors, Biosensors and their Biomedical Applications*, edited by Zhang, X.; Ju, H.; Wang, J., Academic Press: San Diego, 2008. p 158.

(32) Burris, S. C.; Zhou, Y.; Maupin, W. A.; Ebelhar, A. J.; Daugherty, M. W. The Effect of Surface Preparation on Apparent Surface pKa's of ω-Mercaptocarboxylic Acid Self-Assembled Monolayers on Polycrystalline Gold. *J. Phys. Chem. C* **2008**, *112*, 6811–6815.

(33) Serjeant, E. P.; Dempsey, B. Ionisation Constants of Organic Acids in Aqueous Solution. International Union of Pure and Applied Chemistry (IUPAC). IUPAC Chemical Data Series No.23, 1979 Pergamon Press,Inc.: New York, NY.

(34) Morris-Cohen, A. J.; Malicki, M.; Peterson, M. D.; Slavin, J. W. J.; Weiss, E. A. Chemical, Structural, and Quantitative Analysis of the Ligand Shells of Colloidal Quantum Dots. *Chem. Mater.* **2013**, *25*, 1155–1165.

(35) Fu, Y.; Ågren, H.; Kowalewski, J. M.; Brismar, H.; Wu, J.; Yue, Y.; Dai, N.; Thylén, L. Radiative and Nonradiative Recombination of Photoexcited Excitons in Multi-Shell-Coated CdSe/CdS/ZnS Quantum Dots. *EuroPhysics Lett.* **2009**, *86*, 37003.

(36) Fu, Y.; Hellström, S.; Ågren, H. Nonlinear Optical Properties of Quantum Dots - Excitons in Nanostructures,. *J. Nonlinear Opt. Phys. Mater.* **2009**, *18*, 195–226.

(37) Noh, M.; Kim, T.; Lee, H.; Kim, C.-K.; Joo, S.-W.; Lee, K. Fluorescence Quenching Caused by Aggregation of Water-Soluble CdSe Quantum Dots. *Colloids Surf., A* **2010**, *359*, 39–44.

(38) Strating, P.; Wiegel, F. W. Distribution of Ions around a Charged Sphere. *Phys. A* **1993**, *193*, 413–420.

(39) Vosko, S. H.; Wilk, L.; Nusair, M. Accurate Spin-Dependent Electron Liquid Correlation Energies for Local Spin Density Calculations: A Critical Analysis. *Can. J. Phys.* **1980**, *58*, 1200–1211.

(40) Becke, A. D. Density-Functional Exchange-Energy Approximation with Correct Asymptotic Behavior. *Phys. Rev. A: At., Mol., Opt. Phys.* **1988**, *38*, 3098–3100.

(41) Becke, A. D. Density-Functional Thermochemistry. III. The Role of Exact Exchange. *J. Chem. Phys.* **1993**, *98*, 5648–5652.

(42) Lee, C.; Yang, W.; Parr, R. G. Development of the Colle-Salvetti Correlation-Energy Formula into a Functional of the Electron Density. *Phys. Rev. B: Condens. Matter Mater. Phys.* **1988**, *37*, 785–789.

(43) Hehre, W. J.; Ditchfield, R.; Pople, J. A. Self-Consistent Molecular Orbital Methods. XII. Further Extensions of Gaussian-Type Basis Sets for Use in Molecular Orbital Studies of Organic Molecules. *J. Chem. Phys.* **1972**, *56*, 2257–2261.

(44) Barone, V.; Cossi, M. Quantum Calculation of Molecular Energies and Energy Gradients in Solution by a Conductor Solvent Model. *J. Phys. Chem. A* **1998**, *102*, 1995−2001.

(45) Cossi, M.; Rega, N.; Scalmani, G.; Barone, V. Energies, Structures, and Electronic Properties of Molecules in Solution with the C-PCM Solvation Model. *J. Comput. Chem.* **2003**, *24*, 669−681.

(46) Gaussian 09, Revision A.02, Frisch, M. J.; Trucks, G. W.; Schlegel, H. B.; Scuseria, G. E. et al. Gaussian, Inc.: Wallingford CT, 2009.

(47) Perdew, J. P.; Burke, K.; Ernzerhof, M. Generalized Gradient Approximation Made Simple. *Phys. Rev. Lett.* **1996**, *77*, 3865−3868.

(48) Kresse, G.; Hafner, J. Ab Initio Molecular Dynamics for Liquid Metals. *Phys. Rev. B: Condens. Matter Mater. Phys.* **1993**, *47*, 558−561.

(49) Kresse, G.; Hafner, J. Ab Initio Molecular-Dynamics Simulation of the Liquid-Metal-Amorphous-Semiconductor Transition in Germanium. *Phys. Rev. B: Condens. Matter Mater. Phys.* **1994**, *49*, 14251−14269.

(50) Kresse, G.; Furthmüller, J. Efficient Iterative Schemes for Ab Initio Total-Energy Calculations Using a Plane-Wave Basis Set. *Phys. Rev. B: Condens. Matter Mater. Phys.* **1996**, *54*, 11169−11186.

(51) Blöchl, P. E. Projector Augmented-Wave Method. *Phys. Rev. B: Condens. Matter Mater. Phys.* **1994**, *50*, 17953−17979.

(52) Kresse, G.; Joubert, D. From Ultrasoft Pseudopotentials to the Projector Augmented Wave Method. *Phys. Rev. B: Condens. Matter Mater. Phys.* **1999**, *59*, 1758−1775.

(53) Monkhorst, H. J.; Pack, J. D. Special Points for Brillouin-Zone Integrations. *Phys. Rev. B* **1976**, *13*, 5188−5192.